Continuous Modulation of Step Height and Length in Bipedal Walking, combining Reflexes and a Central Pattern Generator*

Philippe Greiner[1], Nicolas Van der Noot[1,2], Auke Jan Ijspeert[2] and Renaud Ronsse[1]

***Abstract*— Deploying humanoid robots in complex and unstructured environments requires the development of efficient and adaptive locomotion controllers. Bio-inspiration holds promises in this perspective, since humans are known to have both an energy efficient gait, and the capacity to modulate it across several features like forward speed and step length and height. In this paper, we report the development of a bio-inspired controller for bipedal walking that can achieve controlled modulations of the step height and length over a large range. This controller builds upon our previous work where we combined both a Central Pattern Generator (CPG) and reflex-like modulations with a layer of virtual muscles providing human-like leg impedance. Here, we report first a sensitivity analysis that was performed to identify those among the many parameters of our controller that can actually modulate the step height and length. Then, we report experimental results illustrating such controlled modulations over a large parameter space.**

I. INTRODUCTION

Nowadays, there are significant research efforts being spent in developing skilled humanoid robots. These robots can be used in a wide variety of situations, ranging from looking through debris in devastated areas [1] to providing support in various tasks of everyday life [2]. Dynamic walking with a bipedal robot can be achieved using several approaches. Among them, those relying on the zero-moment point (ZMP), an indicator of dynamic stability [3], are likely the most popular. However, this approach tends to produce gaits that are energy inefficient, not robust to perturbations and not able to recover after losing balance [4]. These limitations hinder existing robots from being used to their full potential. There is thus a growing need for more human-like bipedal robots, both regarding performance, energy-efficiency and gait modularity.

Locomotion controllers relying on 'Limit Cycle Walking' hold promises in this perspective: the gait is considered as a limit cycle whose global stability is prevalent to its local stability [5]. Bio-inspired bottom-up approaches belong to this category, mainly because they exploit passive dynamics while providing local torque control instead of stiff joint trajectory control. Because they do not require full-featured dynamic models, biological approaches are also less computationally greedy [6]. One of these approaches is the muscle-reflex model developed by Geyer and Herr [7], which embeds bio-relevant force-position and force-velocity relationships, and implements joint torque control by emulating virtual muscles and locomotion reflexes. Interestingly, this model has already been ported to a real humanoid robot [8].

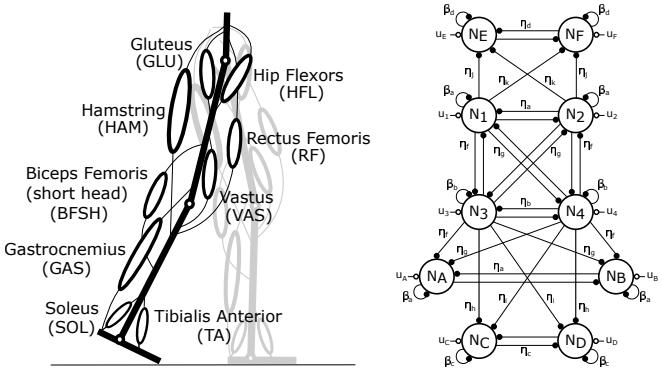

(a) Leg Sagittal Muscles (b) Oscillator Network

Fig. 1: The six Pattern Formation (PF) Neurons N_{A-F} send stimulations to the proximal muscles (HFL, GLU, HAM, BFSH, RF) while the distal ones are only driven by reflexes. HFL and GLU are stimulated by both CPG and reflexes. The four Rhythm Generator (RG) neurons N_{1-4} control the oscillation frequency and coordinate the six PF neurons.

Another control circuitry that is often used in bio-inspired locomotion controllers is the one of central pattern generator (CPG) [4], [9]. A CPG is composed of coupled neural oscillators and generates spatio-temporal patterns of rhythmic activity without external rhythmic inputs. Neurophysiological studies on animals revealed that rhythmic movements are controlled by such networks, typically located in the spinal nervous systems [10], [11].

One of the major issues with existing bipedal robots is their limited capacities regarding gait adaptation and modularity. However, gait modularity is crucial to achieve reliable adaptative locomotion and seamless integration into complex environments. Indeed, navigation through complex and unstructured terrains or obstacles requires not only a robust controller [12], but also the capacity to modulate the gait around its steady-state pattern. For instance, humans are indeed able to adapt their gait to achieve precise foot placement in no more than two steps [13].

Typical contributions achieving precise foot placement in humanoid robotics require kinematic control of the feet

*This research was supported by the Belgian F.R.S.-FNRS (Aspirant #16744574 awarded to NVdN) and by the European Community's Seventh Framework Programme under Grant 611832 (WALK-MAN).

[1]Philippe Greiner, Nicolas Van der Noot and Renaud Ronsse are with the Center for Research in Mechatronics, Institute of Mechanics, Materials and Civil Engineering, and "Louvain Bionics", Université catholique de Louvain, B-1348 Louvain-la-Neuve, Belgium.

[2]Nicolas Van der Noot and Auke Jan Ijspeert are with the Biorobotics Laboratory, Institute of Bioengineering, École Polytechnique Fédérale de Lausanne, CH-1015 Lausanne, Switzerland.

trajectories [14], and generally use stiff motors to actuate the joints [15]. Next to this, bio-inspired approaches also explored the modulation of bipedal gaits, although they typically focused on speed modulation while disregarding other gait features like step height, length, period, or precise foot placement [16], [17], [18], [19]. For instance in [20], we extended the model of [7] with a CPG that featured the capacity of modulating both the locomotion speed, and steering direction. The CPG was mainly activating the proximal hip muscles while the feedback reflexes ruled the activation of the distal ones.

The goal of the present paper is to bridge this gap. More precisely, we report the developments of a bio-inspired controller achieving modular and energy-efficient bipedal locomotion with limited computational cost, in a simulation environment. This locomotion controller builds upon our previous work [19], [20] and runs on COMAN, a humanoid robot which has the size of a 5-year-old child. The main result of this paper is to report step height modulations between 4 and 12cm, and step length modulations between 20 and 50cm, while keeping a stable gait in a very large fraction of this range. We claim that this contribution is a first – yet critical – step towards a bio-inspired bipedal robot achieving precise foot placement and purposeful obstacle avoidance.

The paper is structured as follows. Section II presents the robot that was used as embodiment, in its simulation environment. Section III reports the design of our bio-inspired modulation controller, while Section IV reports the sensitivity analysis that was conducted to identify the modulation parameters. Section V reports the main gait modulation results, and finally Section VI concludes the paper.

II. BIPEDAL EMBODIMENT AND SIMULATOR

The robot used in this contribution is COMAN, developed by the Italian Institute of Technology (IIT). This robot is sized like a 5-year-old child: it is 95cm tall and weighs 31kg. It has 23 controlled degrees of freedom (DOF), equipped with compliant joints implemented using series elastic actuators [21]. Each joint has position, velocity and torque sensors. The robot also features an inertial measurement unit (IMU) and 6-DOF feet force and torque sensors measuring ground reactions [19]. COMAN was modeled and simulated in the Robotran environment. This simulation environment models sensory noise, in an effort to minimize the gap between simulation and reality (see [20], [22] for details). Importantly, the inputs available to the simulated robot are the same as the ones available on the real one. In the context of this work, the simulated robot was constrained to move in the sagittal plane only, similarly to [19].

III. CONTROLLER DESIGN

The robot is controlled using a bio-inspired controller, extensively reported in [19] and [20]. This section overviews this earlier work and highlights the extensions that we provided to achieve step height and length modulations. Here, only the leg *sagittal* DOFs were actuated, and the robot was constrained to move in this plane only (i.e. 2D walking). The particular phase of gait initiation is described in [12].

A. Musculoskeletal model

The key principle of the controller governing the leg sagittal DOFs is to capture muscle groups actuating each leg. These muscle groups (called Muscle-Tendon Units – MTU) receive stimulations, and thus virtually contract in order to actuate the robot joints [7], [20], [23]. The 9 muscles groups used to control COMAN are represented in Fig. 1a.

Obviously, the real or simulated COMAN has no muscle. Instead, virtual muscles are simulated. These muscles are virtually attached to the robot legs, and thus generate forces and torques on the joints when contracting. The simulated (or real) robot can then be actuated to follow the joint torques provided by each of these muscle groups. All the mathematical developments related to this model can be found in [7], [24]. More information related to the MTU state iteration scheme, state initialization, and integration time step can be found in [20].

As compared to the original model [7], two muscles groups were added in the latest version of the controller [23]: the Biceps Femoris short head (BFSH) and the Rectus Femoris (RF). These muscles both act on the knee joint (the BFSH is mono-articular, while the RF also spans over the hip joint), in order to facilitate its flexion, and thus foot clearance. The muscles characteristics used for the BFSH and RF are reported in Table I, the other muscle groups use the same parameters as in [20].

TABLE I: Parameters of the two newly introduced muscles. See [20] for the description of these parameters.

	BFSH	**RF**		**BFSH**	**RF**
F_{max} **[N]**	124	425	r_o **[cm]**	1.708	2.562
v_{max} $[l_{opt}/s]$	18.36	18.36	φ_{max} **[deg]**	-	15
l_{opt} **[cm]**	5.1	3.4	φ_{ref} **[deg]**	20	55
l_{slack} **[cm]**	4.3	14.9	**m [kg]**	0.03	0.12
ρ **[-]**	0.7	0.5 (k) 0.3 (h)	λ **[-]**	0.67	0.423

B. Reflexes and Central Pattern Generator

The signals stimulating the muscle-tendon units are generated both by reflexes (i.e. feedback-driven modulations depending on joints positions, velocities or torques, and on the trunk reference lean angle Θ) and by a Central Pattern Generator (CPG). The rules governing the reflexes are the same as in [19], and hence not detailed here. The CPG model (see Fig. 1b) is adapted from [20], and relies on 10 neurons generating rhythmic patterns. N_1, N_2, N_3 and N_4 are called Rhythm Generation (RG) neurons [25] and provide the fundamental clock of the CPG. The 6 other neurons, denoted with letters, are called Pattern Formation (PF) neurons [25]. They are used to construct the stimulation patterns for the different muscles.

The firing rate x_i of each neuron N_i of this network obeys a state equation similar to the one of a Matsuoka oscillator

[26], [27], with the subscript i corresponding to Fig. 1b:

$$\dot{x}_i = \frac{1}{\tau}(-x_i - \beta_j v_i \quad -\sum_{1}^{3} \eta_k [x_l]^+ + u_i) \tag{1}$$

In Eq. (1), v_i is the self-inhibition state variable, modulated by a gain β_j, u_i is an external tonic excitation feeding each neuron, and τ is the time constant of the CPG. The connection strengths η_k tune the antagonistic inhibitions, i.e. the fact that activation of a given neuron decreases when the antagonistic one is active. The function $[\bullet]^+$ saturates to zero if its argument is negative (i.e. $[x]^+ = max(0,x)$). This captures the fact that neurons can only inhibit each other.

The self-inhibition state dynamics are computed with:

$$\dot{v}_i = \frac{1}{\gamma_j \tau}(-v_i + [x_i]^+) \tag{2}$$

where γ_i is another parameter modulating the self-inhibition time constant. Our CPG network obeys a mirror symmetry reproducing the symmetry of the right and left legs of the robot. The outputs of the CPG are blended to provide stimulations for the leg proximal muscles, as reported in the appendix.

C. Gait optimization

The gait generator reported in the previous sections has many open parameters, that need to be carefully tuned in order to produce the desired gait pattern. This section first describes the step height and step length metrics, and then reports an optimization process and the associated fitness function that were used to achieve this tuning using both of these metrics.

1) Step height and step length metrics: The step height, or ground clearance, is understood as the distance between the swing foot and the ground when the heel of both feet are on the same vertical line during the swing phase (red dashed line in Fig. 2). The resulting height corresponds to the minimal distance between the foot and the ground (i.e. the vertical distance to the toes or heel), displayed with the letter 'H' in Fig. 2. The step length is understood as the distance between two consecutive foot strikes, as displayed with the letter 'L' in Fig. 2.

2) Optimisation and fitness function: The algorithm that we used to achieve the tuning of the controller gains is a Particle Swarm Optimization (PSO) [28], based on the one implemented in [19]. It is an iterative and heuristic optimization method, based on the evaluation of a fitness function over a series of sampled points, distributed within the parameter space. The fitness function used for the optimization was separated in stages, i.e. the next stage was activated when a minimal condition was met with the previous stage.

The first optimization stages were identical to those of [19], and are used to guarantee that the robot walks a minimum distance without falling, while maximizing its walking time. Then, two new fitness stages were introduced, and computed in parallel: the step height and step length stages. These two fitnesses were computed using Gaussian

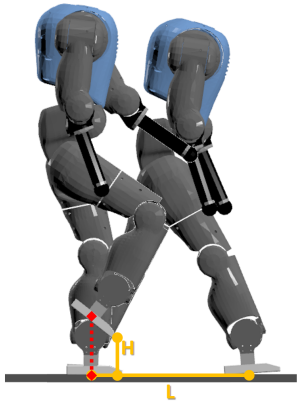

Fig. 2: Representation of the step height 'H' and step length 'L' metrics.

fitness functions like $e^{-\kappa \Delta_l^2}$ where Δ_l (resp. Δ_h) captures the difference between the measured mean step length (resp. step height) and the desired one. The parameter κ modulates the width of the Gaussian. We took it equal to 200 (resp. 2000) for the fitness stage related to step length (resp. step height). The final stages were unlocked when $\Delta_l < 3 \cdot 10^{-2}$ $[m]$ and $\Delta_h < 1 \cdot 10^{-2}$ $[m]$. These two final stages were, again, the same as in [19], i.e. minimizing the virtual metabolic energy spent by the muscles, and minimizing also the phase error between the oscillating neurons and specific gait events. These last stages respectively encouraged human-like muscle-activation patterns, leading to energy-efficient gaits, and proper synchronization between the feed-forward pattern provided by the CPG and the corresponding gait events. In order to encourage gait stability, each optimization was run three times, with the resulting fitness computed as a mean of the three fitnesses.

IV. SENSITIVITY ANALYSIS

Given the large number of open parameters in the gait controller outlined in Section III, it is essential to carefully identify those that will have a significant effect in modulating the gait features of interest (here, step height and length). This section details the sensitivity analysis that was performed to determine and select the relevant parameters for this modulation.

A. Methods

A sensitivity analysis first requires the definition of a so-called reference gait. The parameters corresponding to this reference gait will serve as center of the parameters space being explored in the analysis. Here, we chose a reference gait with a step length of 40 $[cm]$ and a step height of 6.5 $[cm]$. These features were taken from those of a healthy human adult gait [29], [30], scaled to the size of COMAN.

The first parameter optimization was thus conducted in order to have the robot converging to these gait features, according to the method outlined in Section III-C. Then, the sensitivity analysis consisted in analysing the influence of several controller parameters on the gait features. Inspired by

our previous results ([19], [20]), we restricted this analysis to the gains k multiplying the CPG outputs (see the appendix), the time constant of the CPG τ, and the trunk reference lean angle Θ . In total, the sensitivity analysis was performed on 12 parameters: τ, Θ, k_{HFL}, k_{GLU1}, k_{GLU2}, k_{HAM1}, k_{HAM2}, k_{HAM3}, k_{BFSH1}, k_{BFSH2}, k_{RF1} and k_{RF2}.

The sensitivity analysis was performed as follows. For each of these 12 parameters, 4 experimental trials where conducted by taking respectively -20%, -10%, $+10\%$, and $+20\%$ of its reference value, and keeping all the others equal to their reference. Each of these experimental conditions was simulated 3 times in a row, and the average step length and height were computed. Note that the experimental variability was due to some random noise included in the simulated sensors and actuators [19]. Next, the best linear fit (in the least-squares sense) was computed for both gait features for each parameter. We thus obtained 12 linear fits for each of both features, and we considered that the parameters having a significant influence on a given gait feature were those whose slope was at least equal to 5% of the largest slope among the 12.

B. Results

The results of the sensitivity analysis are reported in Table II. For each parameter, the slope of the least squares linear regression is given as a percentage of the maximum slope for each gait feature. Parameters with slopes larger than 5% of the maximum slope (shown in grey in the table) are then considered as having a significant impact in modulating the corresponding feature.

Step length was thus considered to be modulated by 5 controller parameters: Θ, τ, k_{HFL}, k_{GLU1}, and k_{HAM2}. Step height was also significantly impacted by 5 parameters: Θ, τ, k_{GLU1}, k_{HAM1}, and k_{HAM2}. Since 4 of them were taken as significant for both features, the sensitivity analysis revealed that a total of 6 controller parameters should be kept for achieving step height and length modulations. Interestingly, the same 6 parameters emerged from [19], this time for modulating the forward speed.

TABLE II: Slope of the linear fit between each tested controller parameter and the corresponding gait feature, as a function of the maximum slope, [%].

	k_{HFL}	k_{GLU1}	k_{GLU2}	k_{HAM1}	k_{HAM2}	k_{HAM3}
Length	5.65	10.78	2.37	1.18	6.57	1.64
Height	0.95	6.79	2.46	5.02	7.43	3.02
	k_{BFSH1}	k_{BFSH2}	k_{RF1}	k_{RF2}	Θ	τ
Length	0.29	0.74	0.02	0.55	100	5.99
Height	0.00	1.96	1.44	1.41	100	88.52

V. GAIT MODULATION

Once the controller parameters having the most significant influence in modulating the step height and length were identified, we conducted another experiment aiming at modulating these parameters over a large range, and using only the desired height and length as controller inputs. Given the robot's dimensions and some preliminary results, the target range was [5; 12] [cm] for the step height and [25; 50] [cm] for the step length. Moreover, we added two more parameters to those selected by the sensitivity analysis for achieving this experiment: k_{RF1} and k_{RF3}. Indeed, they play a significant role in modulating the knee torque, which turned out to significantly influence both targeted gait features.

A. Methods: parametric co-optimization

1) Modulation function: The experiment was set up as follows. Each of the 8 parameters that were allowed to vary (i.e. the 6 revealed by the sensitivity analysis and the two mentioned above) was modulated by a bi-variate second order polynomial. These polynomials took two inputs, i.e. the reference step length S_l and reference step height S_h, and produced a modulated output being equal to:

$$f_i(\Delta_l,\Delta_h) = K_i + L_{10,i}\cdot\Delta_l + L_{01,i}\cdot\Delta_h + L_{11,i}\cdot\Delta_l\cdot\Delta_h + M_{20,i}\cdot\Delta_l^2 + M_{02,i}\cdot\Delta_h^2 \quad (3)$$

where $\Delta_l = S_l - 0.4$ [m] and $\Delta_h = S_h - 0.065$ [m] are the actual modulation parameters, centered around what we considered to be the center of the parameter space, i.e. $S_l = 40[cm]$ and $S_h = 6.5[cm]$.

Finally, a single new optimization was performed to tune both the non-varying controller parameters, and the coefficients of the 8 polynomial functions captured by Eq. (3), over the whole range of step heights and lengths. We called this a "co-optimization", since 85 parameters were concomitantly tuned through this optimization: 48 for the 6 coefficients of the 8 modulated polynomials, 18 non-modulated muscle stimulation gains, 18 fixed gains of the CPG, and 1 initialization parameter (see [20]). One set of controller parameters is thus a single point within this 85-dimensional parameter space.

2) Fitness computation: To evaluate the fitness of one set of these 85 parameters, 40 simulation trials were run. These correspond to 40 equally spaced points in the $\{S_l, S_h\}$ parametric space. The step height S_h indeed covered the range [5; 12] [cm], with a discretization point every 1 [cm]; and the step length S_l covered the range [25; 45] [cm], with a discretization point every 5 [cm]. For each of these 40 trials, the fitness was computed as reported in Section III-C, and finally, the global fitness of this particular set of parameters was taken as the mean of the 40 fitness trials. Note that each trial was limited to 60 walking seconds maximum, or stopped in case the robot fell.

Over the co-optimization process, the 85 parameters were restricted to evolve within bounds that are reported in Table III. The simulation was run 5 times, again to comply with the intrinsic variability of our simulation environment and the heuristic nature of the Particle Swarm Optimization (see Section III-C). The optimization results with the best fitness were kept.

B. Results

In this section, the performances of the resulting modulations are reported, quantified and discussed. All results

TABLE III: 85 parameters that were co-optimized, together with their lower and upper bounds.

	min	max		min	max		min	max		min	max
β			$L_{10,\tau}$	-0.05	0.15	$K_{BFSH,4}$	0.0	12.0	$L_{01,HAM,1}$	18.0	30.0
β_a	4.5	8.0	$L_{01,\tau}$	-0.19	-0.13	$K_{RF,2}$	2.5	12.0	$L_{11,HAM,1}$	-225.0	-175.0
β_b	2.0	4.5	$L_{11,\tau}$	0.26	0.31	modulated CPG			$M_{20,HAM,1}$	90.0	100.0
β_c	2.0	5.0	$M_{20,\tau}$	0.2	0.26	K_Θ	0.12	0.132	$M_{02,HAM,1}$	-1140.0	-1020.0
β_d	3.0	4.5	$M_{02,\tau}$	3.9	4.9	$M_{20,\Theta}$	-1.2	-0.9	$K_{HAM,2}$	3.2	4.2
γ			reflexes			$M_{02,\Theta}$	-21.0	-16.0	$L_{10,HAM,2}$	-4.8	-2.7
γ_a	4.0	6.0	G_{SOL}	0.6	0.9	$L_{10,\Theta}$	0.24	0.38	$L_{01,HAM,2}$	-10.0	-7.0
γ_b	2.0	3.5	$G_{SOL,TA}$	0.3	1.0	$L_{01,\Theta}$	-0.42	-0.34	$L_{11,HAM,2}$	-55.0	-40.0
γ_c	1.0	5.5	$G_{TA,sw}$	1.5	6.0	$L_{11,\Theta}$	-4.1	-3.5	$M_{20,HAM,2}$	-21.5	-17.5
γ_d	2.5	3.5	$G_{TA,st}$	1.5	2.5	K_{HFL}	4.2	5.0	$M_{02,HAM,2}$	8.0	10.0
η			G_{GAS}	0.4	0.8	$L_{10,HFL}$	10.0	13.0	$K_{RF,1}$	1.8	2.8
η_a	4.5	6.0	G_{VAS}	35.0	45.0	$L_{01,HFL}$	45.0	55.0	$L_{10,RF,1}$	10.0	14.5
η_b	4.5	7.0	$L_{TA,sw}$	0.8	0.9	$L_{11,HFL}$	160.0	210.0	$L_{01,RF,1}$	-110.0	-85.0
η_c	2.5	4.5	$L_{TA,st}$	0.6	0.75	$M_{20,HFL}$	75.0	85.0	$L_{11,RF,1}$	-400.0	-350.0
η_d	4.0	6.5	$\phi_{k,th}$	0.0	0.35	$M_{02,HFL}$	-280.0	-240.0	$M_{20,RF,1}$	30.0	36.5
η_e	2.0	3.0	$K_{p,\Theta}$	8.0	14.0	$K_{GLU,1}$	1.3	2.1	$M_{02,RF,1}$	850.0	950.0
η_f	3.0	4.0	$K_{d,\Theta}$	0.2	0.8	$L_{10,GLU,1}$	6.5	8.5	$K_{RF,3}$	1.7	2.7
η_g	4.0	5.0	fixed CPG			$L_{01,GLU,1}$	-8.5	-6.4	$L_{10,RF,3}$	14.0	19.0
η_h	3.7	4.8	$K_{HAM,3}$	0.0	0.3	$L_{11,GLU,1}$	95.0	115.0	$L_{01,RF,3}$	30.0	40.0
η_i	2.5	3.5	$K_{GLU,2}$	0.0	0.3	M_{20_GLU1}	46.0	57.0	$L_{11,RF,3}$	110.0	140.0
η_j	1.0	4.0	$K_{BFSH,1}$	3.0	12.0	M_{02_GLU1}	540.0	600.0	$M_{20,RF,3}$	125.0	155.0
τ			$K_{BFSH,2}$	0.0	0.5	$K_{HAM,1}$	6.9	7.6	$M_{02,RF,3}$	390.0	460.0
K_τ	0.095	0.125	$K_{BFSH,3}$	0.0	12.0	$L_{10,HAM,1}$	10.0	15.0	init: X_{init}	0.03	0.07

report walking trials of maximum 60 seconds. The explored parameter space was enlarged to $[20;\ 50]$ $[cm]$ for the step length, and to $[4;\ 12]$ $[cm]$ for the step height. These were wider ranges than those used for the co-optimization, because we were interested in investigating how the optimized polynomial modulations (3) generalized beyond their initial regression space.

A global overview of the gait modulation performance is provided in Fig. 3. This figure reports gait results obtained with the best set of 85 parameters, i.e. the outcome of the co-optimization process. Importantly, the biped achieved stable walking for all these trials, although the steady-state error in both stabilized gait features was not similar all over the explored space. In particular, Fig. 3 highlights 4 different regions: the central one is where both features were considered to be accurately controlled (i.e. less than 1.5 $[cm]$ of error for the step height and 3 $[cm]$ for the step length); two other regions capture the parameter subspace where only one of both features was considered to be accurately controlled, and the most peripheral region captures the subspace where none was considered to be accurately controlled, according to the same error threshold. This figure reveals that both features were accurately controlled over most of the regression space, since the regions were one or both features were not considered to be accurately controlled were actually outside of the initial optimization range.

Accurate step feature control is actually the most challenging in the region where the references correspond to both small step lengths and high step heights, i.e. the lower right corner of Fig. 3. This region indeed corresponds to a region where the step height error is large (it actually linearly increases with the height reference in this region), while the step length shows both large errors and large variability, thus compromising accurate control.

Finally, we now report steady-state performance of gait

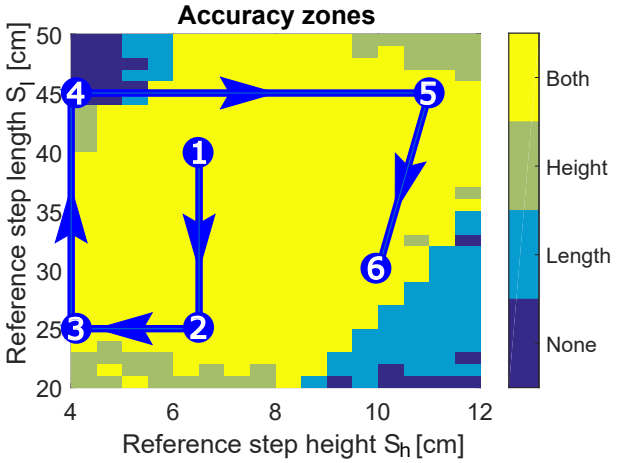

Fig. 3: Graphical representation of parametric regions where the control of step height, step length, or both is accurate. Step height (length) is considered to be accurately controlled if the steady-state error is smaller than 1.5 $[cm]$ (3 $[cm]$), in absolute value. Labels 1 to 6 refer to the successive step features references $\{S_l,S_h\}$ that were applied to the experiment reported in Fig. 4.

features modulation, as well as transitions between these references. More precisely, the robot was requested to modulate its gait along 6 steady-state references reported in Fig. 3. The actual robot performance is reported in Fig. 4. Actual step length was measured between two consecutive foot strikes, and actual step height was measured when both ankles crossed each other. The label displayed as blue circles in Fig. 4 capture the successive $\{S_l,S_h\}$ references provided to the robot controller, consistently to Fig. 3. Each reference stayed stationary for 10 seconds, and each transition lasted 5 seconds in-between. A video of this experiment is provided

as supplementary material (*gait_modulation.mp4*).

The first reference point was $\{S_l,S_h\}=\{40,6.5\}$. This corresponded to the so-called reference gait, i.e. the center of the parametric space explored in the sensitivity analysis reported in Section IV. Fig. 4 reveals that both actual step length and height converged to these values, although minor steady-state errors and moderate fluctuations are also observable. The second reference point was $\{25,6.5\}$, and was applied from $t = 20$ $[s]$. Although the reference step height did not change, its actual value switched from a negative to a positive offset. The step length reached the new smaller reference, with slightly larger variability around steady-state.

The next transition brought the gait to the third reference point, i.e. $\{25,4\}$. This corresponded to the lowest step height reference possible, although the resulting reference pair is still in the "controllable" zone in Fig. 3. Indeed both features correctly converged to their respective references, again with moderate steady-state error and variability. The fourth reference point was $\{45,4\}$. This reference laid in the light blue area in Fig. 3, meaning that step height might be not accurately controlled. Indeed, the step height steady-state error significantly increased of about 2 $[cm]$ over this transition, which incidentally only concerned the step length (switching from 20 to 45 $[cm]$).

The fifth reference point $\{45,11\}$ was located at the boundary of the possible modulation space for step height: although the reference was equal to 11 $[cm]$, the step height oscillated around a significantly smaller value, of about 10 $[cm]$. Finally, the last reference, at $\{30,10\}$, provided again almost no steady-state error, for each of both features. The whole experiment displayed in Fig. 4 also globally reveals that the transitions from one steady-state reference to another were quite fast. Indeed, the gait stabilized around its new steady-state features in less than 2 seconds after all transitions. This corresponds to slightly more than three steps, since one step lasted about 0.65 $[s]$.

In Fig. 5, snapshots of all consecutive foot strikes around the transition from reference 3 to reference 4 are shown. This illustrates that step length indeed progressively increased after the transition in the corresponding reference signal. Similarly, Fig. 6 shows snapshots when step height was measured, for every other step over the transition from reference 4 to reference 5. Again, the figure clearly highlights the evolution in step height from step to step. In particular, the knee and hip joints displayed larger flexion and extension, respectively, in order to produce larger step height.

VI. DISCUSSION AND CONCLUSION

Section IV revealed that 6 parameters of the gait controller played a significant role in modulating the gait features. First, the trunk lean angle Θ had the strongest modulation effect on both the step height and length, and no other parameter reached 10% of these maximum slopes (except the time constant τ for the step height). This result is consistent with all former results obtained with the successive developments of this controller, that all showed a significant influence of this parameter in modulating several gait features [7], [19], [20]. Indeed, the error between the actual trunk angle and this reference amplifies the reflex stimulation partly controlling the GLU and HFL muscle groups, both being proximal MTUs having a strong influence for the whole leg dynamics.

The influence of the CPG time constant τ was also expected to be significant for both features, because step frequency is strongly related to both step length and step height [17], [31]. Our results confirmed this expectation, although the slope was steeper for the step height than for the step length. However, the results obtained while modulating τ should be handled with caution, because most of the negative variations applied to this parameter with respect to its reference value caused the robot to fall. This suggests that the sensitivity of the controller to this parameter might actually be larger than revealed by this linear fit analysis.

The other parameters with significance above the threshold were CPG output gains acting on the HFL, GLU and HAM muscles, i.e. the 3 most proximal MTUs. These 3 muscles indeed actuate the hip (see Fig. 1a), and their resulting torque thus have an impact on the whole leg serial articulated chain. The RF MTU is also connected to the hip, although its gains did not pass the modulation threshold. This was likely due to the fact that this muscle has a lower force capacity F_{max} than the 3 previously mentioned.

In sum, the virtual muscles that received the most significant modulations of their stimulations in order to change the steady-state gait features were all acting on the hip joint. Proximal MTUs are thus likely more critical than distal ones in order to modulate the leg dynamics and thus the associated gait features. This result is consistent with the so-called proximo-distal gradient, postulating that proximal joints and muscles are mainly controlled by descending signals (here the CPG outputs) modulating the gait features, while distal joints and muscles are mainly driven by reflexes (feedback) [9], [20]. This builds upon the rationale that distal muscles are more impacted by external perturbations like ground interactions [32].

The reported experimental gait modulation was able to control – without falling – the gait throughout a parameter space of $[4;\ 12]$ $[cm]$ for the step height and $[20;\ 50]$ $[cm]$ for step length, although small steady-state errors were observed near the boundaries. Taking the size of the COMAN into account, this range is likely approaching the achievable limit of our bio-inspired dynamic walking approach, and actually scales well to the range of a healthy human.

An interesting perspective regarding this modulation could be to analyse the walking speed obtained throughout the modulation space. Indeed, both features being currently modulated do not enable any explicit control of the walking speed. In contrast, modulating the gait period as a third gait feature would leverage the control of the walking speed: step length and period indeed unequivocally determine the walking speed. However, it is expected that modulating a third feature concomitantly with the step height and length will likely induce cross-modulations between them, since only the step height and length already show a certain degree of interdependence.

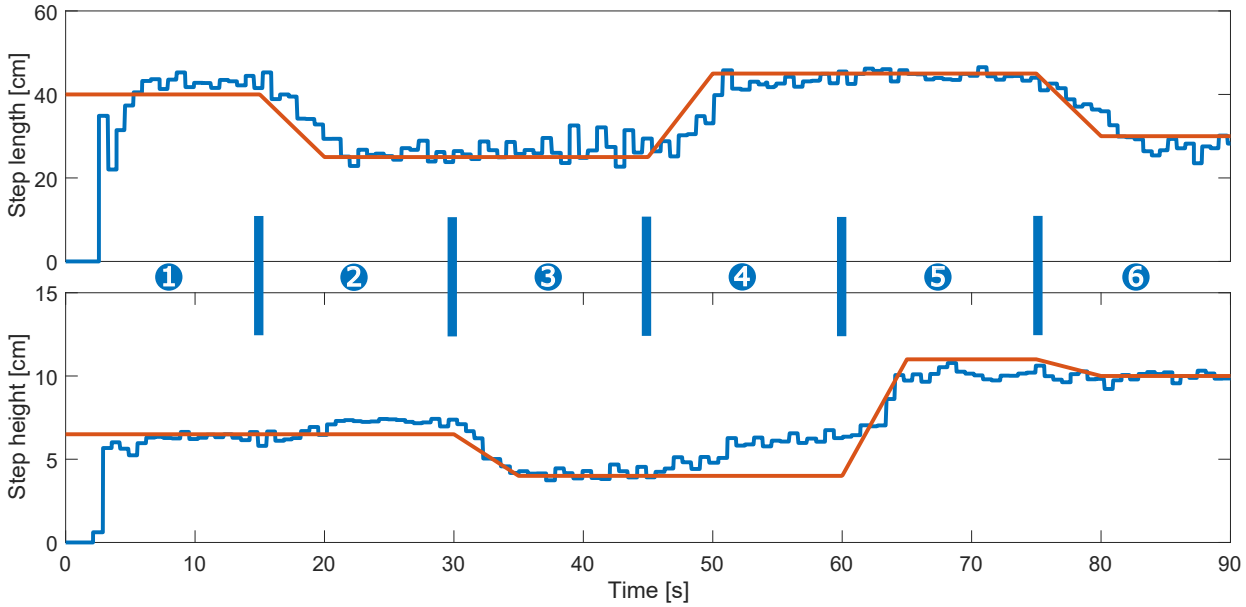

Fig. 4: Actual control of step length and height as a function of time. Both gait features (blue) are plotted with their corresponding reference signal (red). These references switched over 6 different steady-state values being graphically represented in the modulation space in Fig. 3. A video of this experiment is provided as supplementary material (*gait_modulation.mp4*).

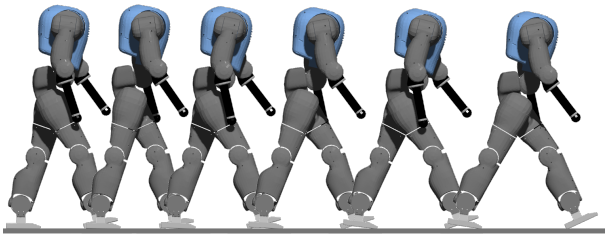

Fig. 5: Transition from reference 3 to 4 (i.e. from $t \approx 47$ $[s]$ to $t \approx 51$ $[s]$), with snapshots taken at each consecutive strike.

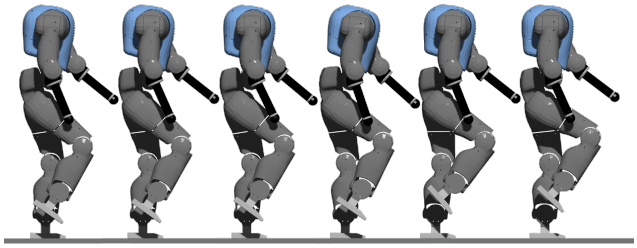

Fig. 6: Transition from reference 4 to 5 (i.e. from $t \approx 58.5$ $[s]$ to $t \approx 66$ $[s]$), with snapshots taken at step height measurement, every other step (when the right foot is in swing).

Another open question regarding our results in whether reducing the steady-state variability of both step features might be achieved. Indeed, estimating the precise foot landing location with our model is currently challenging due to this large step-by-step variability. Better estimation of the foot landing location would be a necessary ingredient towards using our controller for achieving predictive control, and thus selecting the most appropriate reference features according to various potential criteria (e.g. obstacle avoidance, cost of transport, etc.). The step location decision could then be autonomously performed by an appropriate upper-level controller in charge of providing step height and step length references.

Finally, our paper also opens interesting perspectives for investigating the role of descending pathways in the human nervous system. In particular, it would be of interest to report the similarities and differences between the effects of descending modulation from the human spinal cord to the resulting gait, and the mechanisms found here by means of our co-optimization approach.

The present paper paves the way towards the use of humanoid robots achieving both efficient human-like gaits, and accurate control of foot placement through modulation of key gait features. Our future work will consist in extending these results to 3D, i.e. out of the sagittal plane — similarly to [20] for speed and steering modulations — and then porting the same controller to the real hardware. We expect to contribute to the design of robots which efficiently and autonomously navigate through complex environments, thus having the potential of safely interacting with humans, or preventing them from performing hazardous duties.

APPENDIX - MUSCLE STIMULATIONS FROM THE CPG

Proximal muscles are stimulated using the outputs of the CPG neurons according to:

$$\begin{aligned} S_{HFL,R/L} &= k_{HFL} \cdot [y_{2/1}]^+ \\ S_{GLU,R/L} &= k_{GLU1} \cdot [y_{3/4}]^+ + k_{GLU2} \cdot [y_{5/6}]^+ \end{aligned}$$

$$
\begin{aligned}
S_{HAM,R/L} &= k_{HAM1} \cdot [y_{3/4}]^+ + k_{HAM2} \cdot [y_{4/3}]^+ \\
&\quad + k_{HAM3} \cdot [y_{5/6}]^+ \\
S_{BFSH,R/L} &= k_{BFSH1} \cdot [y_{2/1}]^+ + k_{BFSH2} \cdot [y_{5/6}]^+ \\
&\quad + k_{BFSH3} \cdot [y_{3/4}]^+ + k_{BFSH4} \cdot [y_{6/5}]^+ \\
S_{RF,R/L} &= k_{RF1} \cdot [y_{2/1}]^+ + k_{RF2} \cdot [y_{5/6}]^+ + k_{RF3} \cdot [y_{6/5}]^+
\end{aligned}
$$

where R/L stands for right and left, respectively, and $y_i = [[x_j]^+ - [x_k]^+]^+$, with x_j being the firing rate of a PF neuron and x_k the firing rate of a RG neuron directly connected to x_j (see [20]).

REFERENCES

[1] A. Wagoner, A. Jagadish, E. T. Matson, L. EunSeop, Y. Nah, K. K. Tae, D. H. Lee, and J.-E. Joeng, "Humanoid robots rescuing humans and extinguishing fires for Cooperative Fire Security System using HARMS," in *2015 6th International Conference on Automation, Robotics and Applications (ICARA)*, Feb. 2015, pp. 411–415.

[2] Y. Sakagami, R. Watanabe, C. Aoyama, S. Matsunaga, N. Higaki, and K. Fujimura, "The intelligent ASIMO: system overview and integration," in *IEEE/RSJ International Conference on Intelligent Robots and Systems*, vol. 3, 2002, pp. 2478–2483 vol.3.

[3] M. Vukobratović and B. Borovac, "Zero-moment point — thirty five years of its life," *International Journal of Humanoid Robotics*, vol. 01, no. 01, pp. 157–173, Mar. 2004.

[4] A. J. Ijspeert, "Central pattern generators for locomotion control in animals and robots: A review," *Neural Networks*, vol. 21, no. 4, pp. 642–653, May 2008.

[5] D. G. E. Hobbelen and M. Wisse, "Limit Cycle Walking," in *Humanoid Robots, Human-like Machines*, M. Hackel, Ed. Vienna, Austria: I-Tech Education and Publishing, June 2007, pp. 277–294.

[6] T. Luksch, "Human-like control of dynamically walking bipedal robots," Ph.D. dissertation, Technischen Universität Kaiserslautern, 2010.

[7] H. Geyer and H. Herr, "A Muscle-Reflex Model That Encodes Principles of Legged Mechanics Produces Human Walking Dynamics and Muscle Activities," *IEEE Transactions on Neural Systems and Rehabilitation Engineering*, vol. 18, no. 3, pp. 263–273, June 2010.

[8] N. Van der Noot, L. Colasanto, A. Barrea, J. van den Kieboom, R. Ronsse, and A. J. Ijspeert, "Experimental validation of a bio-inspired controller for dynamic walking with a humanoid robot," in *Intelligent Robots and Systems (IROS), 2015 IEEE/RSJ International Conference on*. IEEE, 2015, pp. 393–400.

[9] F. Dzeladini, J. van den Kieboom, and A. Ijspeert, "The contribution of a central pattern generator in a reflex-based neuromuscular model," *Frontiers in Human Neuroscience*, vol. 8, June 2014.

[10] F. Delcomyn, "Neural basis of rhythmic behavior in animals," *Science*, vol. 210, no. 4469, pp. 492–498, Oct. 1980.

[11] G. Taga, "Emergence of bipedal locomotion through entrainment among the neuro-musculo-skeletal system and the environment," *Physica D: Nonlinear Phenomena*, vol. 75, no. 1-3, pp. 190–208, 1994.

[12] F. Heremans, N. Van der Noot, A. J. Ijspeert, and R. Ronsse, "Bio-inspired balance controller for a humanoid robot," in *2016 6th IEEE International Conference on Biomedical Robotics and Biomechatronics (BioRob)*, June 2016, pp. 441–448.

[13] J. S. Matthis, S. L. Barton, and B. R. Fajen, "The critical period for the visual control of foot placement in complex terrain occurs in the preceding step," *Perception and Action Lab, Cognitive Science Dept, RPI, Troy, NY, USA*, 2015.

[14] G. Brunnett, Ed., *Geometric modeling for scientific visualization*, ser. Mathematics and visualization. Berlin ; New York: Springer, 2004.

[15] M. Ceccarelli, *Technology Developments: the Role of Mechanism and Machine Science and IFToMM*. Springer Science & Business Media, May 2011, p.63.

[16] S. Song and H. Geyer, "Regulating speed in a neuromuscular human running model," in *Humanoid Robots (Humanoids), 2015 IEEE-RAS 15th International Conference on*. IEEE, 2015, pp. 217–222.

[17] ——, "Regulating speed and generating large speed transitions in a neuromuscular human walking model," in *Robotics and Automation (ICRA), 2012 IEEE International Conference on*. IEEE, 2012, pp. 511–516.

[18] A. A. Saputra, J. Botzheim, I. A. Sulistijono, and N. Kubota, "Biologically Inspired Control System for 3-D Locomotion of a Humanoid Biped Robot," *IEEE Transactions on Systems, Man, and Cybernetics: Systems*, vol. 46, no. 7, pp. 898–911, July 2016.

[19] N. Van der Noot, R. Ronsse, and A. J. Ijspeert, "Biped gait controller for large speed variations, combining reflexes and a central pattern generator in a neuromuscular model," in *2015 IEEE International Conference on Robotics and Automation (ICRA)*. IEEE, 2015, pp. 6267–6274.

[20] N. Van der Noot, A. J. Ijspeert, and R. Ronsse, "Bio-inspired controller achieving forward speed modulation with a 3d bipedal walker," *The International Journal of Robotics Research*, vol. 37, no. 1, pp. 168–196, Jan. 2018.

[21] G. A. Pratt and M. M. Williamson, "Series elastic actuators," in *Proceedings 1995 IEEE/RSJ International Conference on Intelligent Robots and Systems. Human Robot Interaction and Cooperative Robots*, vol. 1, Aug. 1995, pp. 399–406 vol.1.

[22] A. A. Zobova, T. Habra, N. Van der Noot, H. Dallali, N. G. Tsagarakis, P. Fisette, and R. Ronsse, "Muti-physics modeling of a compiant humanoid robot," *Multibody System Dynamics*, vol. 39, no. 1-2, pp. 95–114, Jan. 2017.

[23] S. Song and H. Geyer, "A neural circuitry that emphasizes spinal feedback generates diverse behaviours of human locomotion: A spinal feedback circuitry generating human locomotion behaviors," *The Journal of Physiology*, vol. 593, no. 16, pp. 3493–3511, Aug. 2015.

[24] H. Geyer, A. Seyfarth, and R. Blickhan, "Positive force feedback in bouncing gaits?" *Proceedings of the Royal Society B: Biological Sciences*, vol. 270, no. 1529, pp. 2173–2183, Oct. 2003.

[25] D. A. McCrea and I. A. Rybak, "Organization of mammalian locomotor rhythm and pattern generation," *Brain research reviews*, vol. 57, no. 1, pp. 134–146, Jan. 2008.

[26] K. Matsuoka, "Sustained oscillations generated by mutually inhibiting neurons with adaptation," *Biological cybernetics*, vol. 52, no. 6, pp. 367–376, 1985.

[27] ——, "Mechanisms of frequency and pattern control in the neural rhythm generators," *Biological cybernetics*, vol. 56, no. 5-6, pp. 345–353, 1987.

[28] J. Kennedy and R. Eberhart, "Particle swarm optimization," in *, IEEE International Conference on Neural Networks, 1995. Proceedings*, vol. 4, Nov. 1995, pp. 1942–1948 vol.4.

[29] T. Oberg, A. Karsznia, and K. Oberg, "Basic gait parameters: reference data for normal subjects, 10-79 years of age," *Journal of rehabilitation research and development*, vol. 30, pp. 210–210, 1993.

[30] F. Dadashi, B. Mariani, S. Rochat, C. J. Büla, B. Santos-Eggimann, and K. Aminian, "Gait and Foot Clearance Parameters Obtained Using Shoe-Worn Inertial Sensors in a Large-Population Sample of Older Adults," *Sensors (Basel, Switzerland)*, vol. 14, no. 1, pp. 443–457, Dec. 2013.

[31] M. P. Murray, R. C. Kory, B. H. Clarkson, and S. B. Sepic, "Comparison of free and fast speed walking patterns of normal men," *ResearchGate*, vol. 45, no. 1, pp. 8–23, Mar. 1966.

[32] M. A. Daley, G. Felix, and A. A. Biewener, "Running stability is enhanced by a proximo-distal gradient in joint neuromechanical control." *The Journal of experimental biology*, vol. 210, no. Pt 3, pp. 383–394, Feb. 2007.